

Boise State University

ScholarWorks

Materials Science and Engineering Faculty
Publications and Presentations

Micron School for Materials Science and
Engineering

3-2021

Interface Structure and Luminescence Properties of Epitaxial PbSe Films on InAs(111)A

Kevin D. Vallejo
Boise State University

Paul J. Simmonds
Boise State University

Publication Information

Haidet, Brian B.; Nordin, Leland; Muhowski, Aaron J.; Vallejo, Kevin D.; Hughes, Eamonn T.; Meyer, Jarod; . . . and Mukherjee, Kunal. (2021). "Interface Structure and Luminescence Properties of Epitaxial PbSe Films on InAs(111)A". *Journal of Vacuum Science and Technology A*, 39(2), 023404-1 - 023404-11.

<https://doi.org/10.1116/6.0000774>

This article may be downloaded for personal use only. Any other use requires prior permission of the author and AIP Publishing. This article appeared in

Haidet, B.B.; Nordin, L.; Muhowski, A.J.; Vallejo, K.D.; Hughes, E.T.; Meyer, J.; . . . & Mukherjee, K. (2021). Interface Structure and Luminescence Properties of Epitaxial PbSe Films on InAs(111)A. *Journal of Vacuum Science and Technology A*, 39(2), 023404.

and may be found at <https://doi.org/10.1116/6.0000774>

Interface structure and luminescence properties of epitaxial PbSe films on InAs(111)A

Cite as: J. Vac. Sci. Technol. A 39, 023404 (2021); doi: 10.1116/6.0000774

Submitted: 10 November 2020 · Accepted: 30 December 2020 ·

Published Online: 27 January 2021



Brian B. Haidet,¹ Leland Nordin,² Aaron J. Muhowski,² Kevin D. Vallejo,³ Eamonn T. Hughes,¹ Jarod Meyer,⁴ Paul J. Simmonds,^{3,5} Daniel Wasserman,² and Kunal Mukherjee^{1,4,a)}

AFFILIATIONS

¹Materials Department, University of California, Santa Barbara, California 93106

²Electrical and Computer Engineering Department, University of Texas, Austin, Texas 78705

³Micron School of Materials Science and Engineering, Boise State University, Boise, Idaho 83725

⁴Department of Materials Science and Engineering, Stanford University, Stanford, California 94305

⁵Department of Physics, Boise State University, Boise, Idaho 83725

Note: This paper is part of the Special Topic Collection: Honoring Dr. Art Gossard's 85th Birthday and his Leadership in the Science and Technology of Molecular Beam Epitaxy.

a) Author to whom correspondence should be addressed: kunalm@stanford.edu

ABSTRACT

Epitaxial heterostructures of narrow-gap IV-VI and III-V semiconductors offer a platform for new electronics and mid-infrared photonics. Stark dissimilarities in the bonding and the crystal structure between the rocksalt IV-VIs and the zincblende III-Vs, however, mandate the development of nucleation and growth protocols to reliably prepare high-quality heterostructures. In this work, we demonstrate a route to single crystal (111)-oriented PbSe epitaxial films on nearly lattice-matched InAs (111)A templates. Without this technique, the high-energy heterovalent interface readily produces two populations of PbSe grains that are rotated 180° in-plane with respect to each other, separated by rotational twin boundaries. We find that a high-temperature surface treatment with the PbSe flux extinguishes one of these interfacial stackings, resulting in single-crystalline films with interfaces that are mediated by a monolayer of distorted PbSe. While very thin PbSe-on-InAs films do not emit light, hinting toward a type-III band alignment, we see strong room temperature photoluminescence from a 1.5 μm thick film with a minority carrier lifetime of 20 ns at low-excitation conditions and bimolecular recombination at high excitation conditions, respectively, even with threading dislocation densities exceeding 10⁸ cm⁻². We also note near-complete strain relaxation in these films despite large thermal expansion mismatch to the substrate, with dislocations gliding to relieve strain even at cryogenic temperatures. These results bring to light the exceptional properties of IV-VI semiconductors and the new IV-VI/III-V interfaces for a range of applications in optoelectronics.

Published under license by AVS. <https://doi.org/10.1116/6.0000774>

I. INTRODUCTION

IV-VI semiconductors like PbSe have long been candidate materials for mid-infrared optoelectronics^{1–6} thanks to their tunable narrow direct bandgaps, reduced bulk Auger recombination coefficient, high refractive indices, and tolerance to charged defects due to their high dielectric constants⁶ and bonding character.^{7–9} A majority of studies on IV-VI devices have involved epitaxial growth on native IV-VI (rocksalt) or ionic BaF₂ (fluorite) substrates and buffer layers, which have a number of drawbacks including poor thermal performance, low mechanical stability, and,

in the case of fluorite substrates, small size and difficult processing due to solubility in water. This has prompted research into IV-VI growth on silicon^{10–12} and III-V substrates like GaAs or InSb,^{13–16} sometimes with II-VI buffer layers.^{17–20} The zincblende-structured III-V substrates offer better crystalline and surface quality, lattice constant matching, mechanical strength, chemical stability, and thermal conductivity compared to fluorite or native IV-VI rocksalt substrates. IV-VI/III-V heteroepitaxy, however, is not without its challenges. The IV-VI/III-V interface incorporates drastic changes in bonding character, valency, crystal structure, and surface charge,

factors that contribute to very high interfacial energies and result in a difficult-to-control and defect-prone 3D island growth mode in the early stages. Success in developing epitaxial tools to prepare sharp (and necessarily metastable) IV-VI/III-V interfaces reliably enables harnessing of these material dissimilarities for new means to access the unique mid-infrared optical properties of IV-VI materials as well as for the creation and control of novel interfacial electronic phenomena.¹⁹

In addition to preparing the interface, we need to consider the choice of growth orientation in IV-VI/III-V heterostructures. The IV-VI rocksalt structure preferentially facets on the {001} family of planes, making (001) a favored growth direction. This would have been an attractive feature given that (001) III-V molecular beam epitaxy (MBE) growth is well established. Unfortunately, (001)-oriented IV-VI rocksalts lack the ability to relax strain from lattice or thermal mismatch via a dislocation glide. Unlike most ionic rocksalts,²¹ the IV-VI rocksalts' primary slip system is {001}⟨110⟩, meaning typical dislocation burgers' vectors lie in ⟨110⟩ directions and dislocations glide on {001} planes. Consequently, this slip system feels no resolved shear stress from in-plane strain on an (001)-oriented film,²² and thermally mismatched IV-VI films readily crack upon cooldown,^{10,11} even when cooling from low growth temperatures.

The handicap of the PbSe slip system becomes an asset when growing IV-VI films oriented in the (111) direction. The primary slip system of the rocksalt IV-VIs, when active, has very low energy barriers to the dislocation glide.²¹ Amazingly, dislocations glide even at cryogenic temperatures, permitting full relaxation²³ and allowing for annihilation of dislocations during growth with high efficiency.²² The ability to access this slip system enables (111)-oriented IV-VI structures to be grown thicker without cracking, to be improved via thermal cycling, and to be temperature-tunable without inducing strain to a device.

In this paper, we explore PbSe/InAs(111)A heteroepitaxy. We demonstrate control over the interfacial structure and characterize structural defects, film relaxation, and minority carrier recombination behavior of the (111)-oriented PbSe film. Although these two materials are nearly lattice matched (1.1% mismatch at room temperature), their (111) heterointerface has not been previously investigated. We observe typical polycrystalline nucleation that can be actively controlled via a surface treatment to produce single-crystal films. We characterize two distinct interfaces that can occur between these materials via high resolution scanning transmission electron microscopy and measure photoluminescence (PL) from single-crystal PbSe/InAs at room temperature. These PL results enable the probing of both mechanical behavior in the form of thermal mismatch relaxation and electronic behavior in the form of minority carrier lifetime and dominant recombination mechanisms.

II. METHODS

We started with commercially available, nominally on-axis ($\pm 0.5^\circ$) InAs(111)A substrates that are unintentionally doped n-type, with carrier concentrations of $1\text{--}3 \times 10^{16} \text{ cm}^{-3}$. To ensure high-quality surfaces for subsequent growth, we grew 100 nm InAs (111)A buffers in a GEN 930 MBE system using elemental indium

and As₄ sources.²⁴ We capped the InAs buffers with an amorphous arsenic layer for out-of-vacuum transport into a separate Riber Compact 21 MBE system configured for IV-VI growth. In the IV-VI chamber, the amorphous arsenic was thermally desorbed to recover the bare III-V epi-surface. PbSe films were then grown on the InAs(111)A buffers using a compound PbSe cell. We primarily focus on a 1.5 μm thick film of PbSe(111) for structural and optical characterization and additionally use 65 nm thick films to learn about the nucleation process.

The PbSe growth procedure was informed by our previous work on InAs(001) substrates where we extinguished competing {110} and {221} PbSe nuclei orientations and produced single-crystalline PbSe(001) films via a two-step process: (i) exposing the substrate to the PbSe flux from a compound PbSe effusion cell above the PbSe re-evaporation temperature (380–400 °C) followed by (ii) PbSe nucleation and growth at a lower temperature (300–330 °C).¹⁶ On InAs(001) films, we observed the surface reconstruction change to 2×1 as a result of this dose.

The InAs(111)A buffers in this study were similarly exposed to the molecular PbSe flux from a compound source at elevated temperature: approximately 3×10^{-7} Torr of the PbSe flux for times ranging from 30 s to 25 min and at temperatures ranging from 360 °C to 460 °C. The surface reconstruction was observed using reflection high energy electron diffraction (RHEED) to adopt a 1×1 pattern after the dose. Samples were then cooled to 280–330 °C and the compound PbSe flux was reinitiated to grow the PbSe film.

Plan-view scanning electron microscopy (SEM) and electron channeling contrast imaging (ECCI) micrographs were recorded on an FEI Apreo S and an FEI Apreo C. Samples were prepared for scanning transmission electron microscopy (STEM) via a focused ion beam-liftout process in an FEI Helios Dualbeam system. The sample from Fig. 4(b) utilized a FIB polishing process to produce a smooth, sloped surface, and then ECCI was performed on the slope to see plan view diffraction contrast at varying depths in the film. Cross-sectional STEM analysis was completed on an FEI Talos STEM, utilizing annular dark field (ADF) and high-angle annular dark field (HAADF) detectors. X-ray diffraction (XRD) experiments were executed on a Panalytical MRD PRO system utilizing the monochromator for high-resolution coupled scans and rocking curves.

The total emission from the samples was measured using a microphotoluminescence setup. The sample is held in a temperature-controlled cryostat with a ZnSe window. The sample is optically pumped by a 808 nm laser outputting 1 W and modulated at 10 kHz. The pump laser light is passed through a 3 μm dichroic beamsplitter and focused onto the sample using an all-reflective objective. PL emitted from the sample is collected by the same objective and reflected by the dichroic beamsplitter. The reflected light is focused by a reflective parabolic mirror through an AR-coated (3–5 μm) Si window onto a liquid nitrogen cooled HgCdTe detector. The Si window is used to filter laser light. The detector signal is demodulated by a lock-in amplifier and recorded for each temperature of the sample. For spectrally resolved photoluminescence measurements, infrared light is passed into a Fourier transform infrared (FTIR) setup after being reflected from the dichroic. The FTIR is run in the step-scan mode to dramatically

reduce infrared background. The input power was approximately 240 mW, focused into an ellipse of $200 \times 40 \mu\text{m}^2$.

In addition, we also perform time-resolved photoluminescence (TRPL) measurements on all of our materials. In these measurements, the sample is again housed in a low temperature cryostat and excited with a pulsed ($<1 \text{ ns}$) 532 nm laser with $1.3 \mu\text{J}$ pulse energy and 10 kHz repetition rate. Emission is collected with a parabolic mirror and then focused onto a high speed Vigo MCT detector. The InAs band edge emission is filtered with a $3.6 \mu\text{m}$ long pass filter before the detector. Pulse energy is controlled using neutral density filters. The detector signal is collected and averaged using a LeCroy 12-bit high speed oscilloscope.

Bandgap was estimated via PL by fitting to locate the peak emission energy and subtracting $\frac{1}{2}kT$. Data surrounding the CO_2 absorption peak were not included in the peak fit, and near-room-temperature results were not included in the bandgap versus the temperature analysis because the CO_2 absorption was significantly overlapping the emission, artificially shifting the maximum.

III. RESULTS

A. Heterovalent interface formation

We find that deposition of PbSe on InAs(111)A frequently results in polycrystalline nuclei, but single crystalline films can be obtained via proper application of the high-temperature surface treatment described above. The films in Figs. 1(a) and 1(c) are both 65 nm PbSe films that received different surface treatments. The film in Fig. 1(a) has nanoscale rotated/mirrored grains, while the film in Fig. 1(c) is single-crystalline, with only threading dislocations visible to ECCI.

The polycrystalline film [Fig. 1(a)] was grown on an InAs substrate treated with PbSe flux at 360°C for 15 min, but this substrate temperature was too low and the RHEED pattern became spotty during the dose. When growth was reinitiated at 320°C , triangular nanoscale grains were observed [Figs. 1(a) and 1(b)]. We believe that this substrate temperature was not far enough above the evaporation temperature for PbSe, and some PbSe was deposited on the substrate in the form of very small islands, which acted as seeds for later deposition.

The single-crystalline film [Fig. 1(c)] was grown on an InAs substrate treated with PbSe flux at 400°C for 15 min. During this dose, the surface reconstruction transitioned smoothly from a 2×2 to a 1×1 and remained streaky, indicating that a smooth surface was maintained while the surface structure was altered. Subsequent growth on this smooth altered surface at 320°C resulted in single-crystalline films. Later experiments showed that a 400°C surface treatment is effective after only 30 s, so at a high temperature, a relatively short surface treatment is sufficient to chemically and structurally prepare the surface for single-orientation growth.

In order to determine the mechanism behind this dosing procedure, we examined these interfaces in more detail. The PbSe film shown in Fig. 1(a) is the result of uncontrolled competition between two distinct interfacial stackings that are 180° rotated with respect to one another but share the [111] direction with the substrate. One of these orientations shares threefold rotational

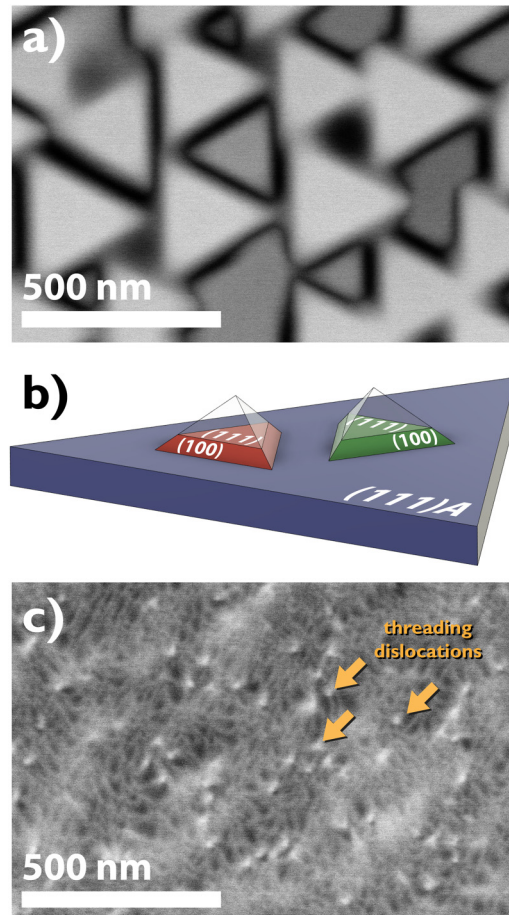


FIG. 1. Surface treatment eliminates twins (180° rotated grains) in (111) oriented PbSe films: ECCI micrographs show 65 nm thick films of PbSe grown on InAs at 320°C with different pretreatments. (a) A film receives a 15 min dose at 360°C and shows two populations of triangular grains with shallow trenches between them marking twin boundaries. (b) Schematic of the rotations in cubic symmetry observed in the film (a). (c) A film receives a 15 min dose at 400°C and shows a single-orientation structure with some dislocations. Note that (c) is processed with significantly higher contrast than (a).

symmetry with the substrate (the so-called “type A” epitaxy), while the other is reversed, effectively making the entire heterointerface a rotational twin (“type B” epitaxy). The preferred triangular habit of the coalesced islands, along with the dark/light orientational contrast provided by ECCI, reveals their internal structure [Fig. 1(b)]. The heterovalent interface between InAs(111)A and PbSe(111) appears to be very high-energy, and consequently, heteroepitaxy occurs in the Volmer-Weber growth mode of island nucleation and coalescence. Like-facing grains coalesce evenly, likely forming misfit and threading dislocations during island fusion, but in the more extreme case of oppositely rotated grains, coalescence results in a twin boundary marked by a shallow trench in the film’s surface. For this reason, controlling the nominal orientation of

every island with respect to the substrate is essential for high-quality crystal growth.

We have characterized both of these interfacial stackings (unrotated, type A, and rotated, type B) using HR-STEM in Fig. 2. Atomic columns were identified via relative HAADF contrast. The primary difference between the A and B stackings is the placement of the first layer of lead atoms: in the type A interface, these lead atoms are lined up directly above the top layer of arsenic in the substrate, while in the type B interface, the lead and arsenic are farther apart. In both cases, the bond angles around the first layer of lead atoms define the threefold cubic symmetry for the rocksalt film. We believe that during our high-temperature surface pretreatment, we are giving this first layer of lead atoms the kinetic freedom to migrate to the energetically favorable A or B site. Interestingly, this equilibrium structure achieved in Fig. 1(c) is actually type B epitaxy—it seems counterintuitive that the creation of a rotational twin across an already expensive heterointerface could be energetically favored.

A more detailed analysis of the interface in Fig. 2 shows some slight distortions at the interface, the most dramatic of which is the spacing of the first PbSe monolayer. Although actual lattice distortions are likely more nuanced, a tentative interpretation of the interplanar spacings near the interface [Fig. 2(c)] indicates that the first layer of PbSe in both structures is nearly a zincblende-ordered monolayer of PbSe. If this interpretation is correct, there is a slight separation between the chemical heterointerface and the structural heterointerface. During the high-temperature dose at 400 °C, the PbSe evaporation rate is high and only a single monolayer can adhere to the substrate. In the absence of more rocksalt layers, the

most stable conformation for the PbSe monolayer is to continue the existing tetrahedrally coordinated zincblende lattice. When this pseudozincblende monolayer is cooled to ~300 °C and PbSe growth is initiated, the first layer of lead atoms assumes its octahedral rocksalt coordination, and the bond angles of this lead layer set the symmetry for the rest of the PbSe film.

B. Propagation of substrate twins

A PbSe film free of grains would be ideal, but homoepitaxial growth of InAs(111)A is still under development and the InAs buffer layers used in this work contain some twins that are transmitted up to the PbSe films. It is worth clarifying that these boundaries are between twinned grains of the PbSe crystal. As PbSe has threefold rotational symmetry about the [111] direction and mirror planes parallel to the [111] direction, the structure on one side of one of these boundaries can accurately be considered either rotated or mirrored with respect to the structure on the other side. The vertical boundaries we observe are frequently not in symmetric directions and so may be largely incoherent. While not perfect substrates for devices, these differing grains present on the same sample surface actually provide an excellent test of robustness for the high-temperature dose mechanism.

Figure 3 shows how large twinned grains in the substrate are propagated through the heterointerface to the PbSe film. In Fig. 3(a), we see two twin boundaries in the InAs buffer (with a third below the imaged frame). One of these twin boundaries curves to intersect the heterointerface. On the left, an InAs layer that shares cubic symmetry with the substrate grows 180° rotated

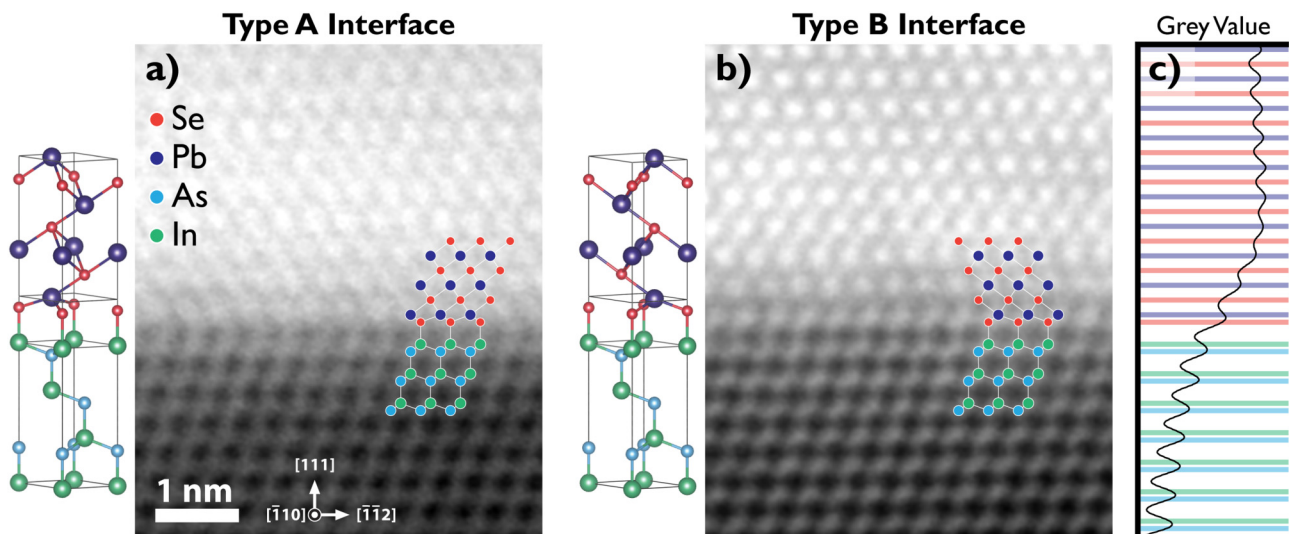


FIG. 2. PbSe/InAs interfacial structures: High-resolution HAADF-STEM cross sections of two PbSe/InAs interfaces with proposed structures. Reconstructed structures assume threefold rotational symmetry in the growth plane. (a) The metastable type A cross section was cut from a stacking-fault-free region of the PbSe/InAs interface from a sample that received an ineffective surface treatment [Fig. 1(a)]. (b) The equilibrium type B cross section was cut from a sample treated with the PbSe flux at 400 °C where all PbSe/InAs interfaces include exactly one rotational twin, resulting in a 180° rotated film. A wide integrated line trace (c) of the type B interface HAADF image is also shown to demonstrate regular interplanar spacings through the interface, with the first layer of PbSe compressed toward zincblende. (STEM Processing details: 20 images, stacked for drift correction, smoothed with $\alpha = 200$ pm gaussian blur.)

PbSe, forming a heteroepitaxial rotational twin. On the right, a 180° rotated InAs layer acts as a substrate for 0° rotated PbSe, similarly forming a rotational twin, but resulting in a film that shares threefold symmetry with the substrate. The boundary then continues vertically between the left and right grains of PbSe, producing a wide moiré pattern in the center of the image.

Figure 3(b) shows a wider view of one of these boundaries in darkfield STEM. The twinning in the InAs substrate is close enough to the interface that it is nearly invisible at this scale, but the twin boundary in the PbSe is bright and grows upward vertically until intersecting the surface, where a shallow trench has formed between the grains. Interestingly, this trench is also highly crystallographic and opens with faces $\sim 36^\circ$ to vertical, indicating mirrored (001) planes form the internal faces of the trench.

The grain structure in these PbSe films inherited from the InAs substrate is quite large, with typical faulted regions spanning tens of micrometers. Figure 3(c) shows a plan-view ECCI micrograph of a 65 nm PbSe film—we believe that the majority of the film (dark contrast) does not have rotational twins in the buffer and is then 180° rotated to the substrate, while the pockets of light contrast are grown on the rotated/mirrored buffer and share symmetry with the substrate.

C. Film quality and relaxation

Via ECCI, we observe vertical twin boundary density of approximately $1 \times 10^3 \text{ cm}^{-1}$ and a threading dislocation density (TDD) of $7 \times 10^9 \text{ cm}^{-2}$ in 65 nm thick PbSe layers [Fig. 1(c)]. In the thicker $1.5 \mu\text{m}$ film, this defect density drops precipitously: we measure a TDD of $1.6 \times 10^8 \text{ cm}^{-2}$ via plan-view TEM a couple hundred nanometers below the surface, and approximately $1 \times 10^8 \text{ cm}^{-2}$ just below the top surface via ECCI, across both populations of grains. With thermal cycling, etch pit density (EPD) in $4 \mu\text{m}$ thick PbSe(111) on silicon has been previously reported as low as 10^6 cm^{-2} .²² The reported lower TDD in these earlier works is partly explained by the thicker film and higher thermal expansion mismatch between PbSe and Si (leading to more efficient dislocation filtering during cyclic annealing), but our observation of dislocation clustering via ECCI and STEM suggests that EPD may also underrepresent TDD. TDDs of 10^7 – 10^8 cm^{-2} have been measured for $4 \mu\text{m}$ films of PbTe(111)/BaF₂ via scanning tunneling microscopy,²⁵ aligning closely with our results. We further characterize the structural relaxation of these materials via XRD and PL.

At room temperature, XRD measurements of the (444) peak of PbSe show that the $1.5 \mu\text{m}$ PbSe film is fully relaxed within

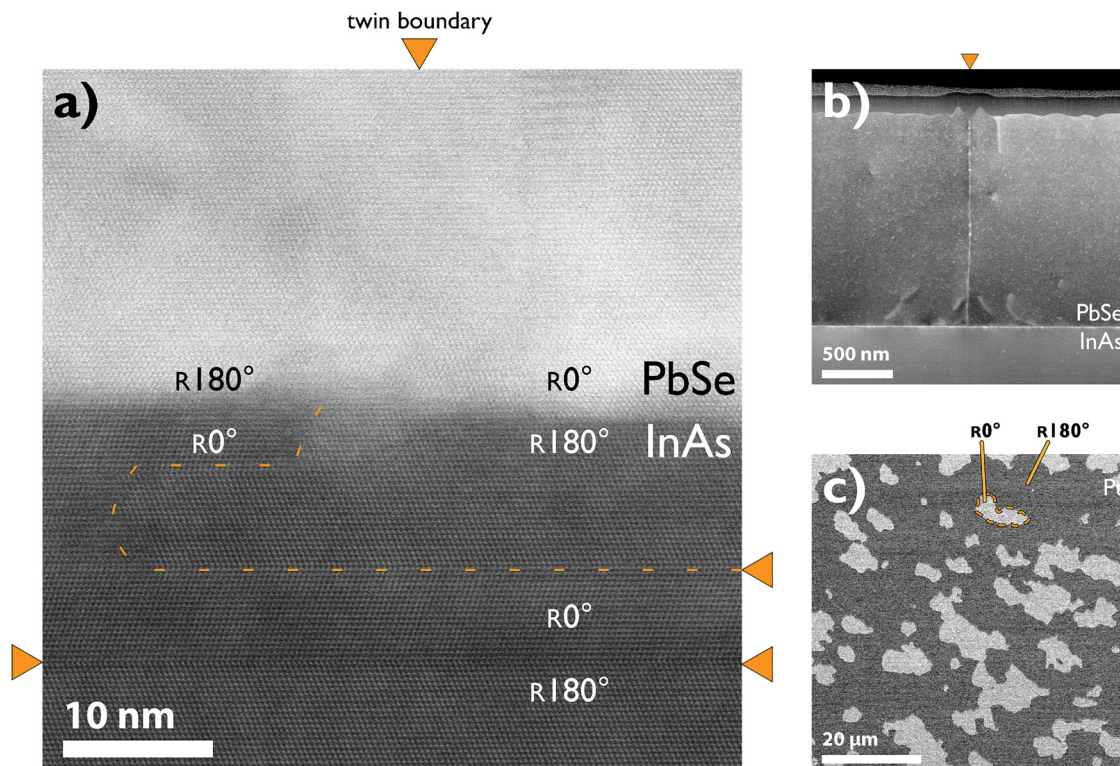


FIG. 3. Subsurface twins in InAs can propagate into the PbSe film: (a) HR HAADF-STEM of a twin boundary in the InAs buffer intersecting the heteroepitaxial interface and inducing a twin boundary in the $1.5 \mu\text{m}$ PbSe film. (b) ADF-STEM of a twin boundary in a PbSe film, terminating in a faceted trench at the film surface. (c) Plane-view ECCI micrograph of the 65 nm PbSe film with rotated/mirrored grains originating in the buffer layer. [Processing details: (b) denoised with a 2px median filter, (c) smoothed with $\alpha = 1 \mu\text{m}$ gaussian blur.]

the measurement limits of the high-resolution diffractometer used [Fig. 4(a)]. Calibrating to a predicted InAs (444) spacing of 0.8744 Å, we observe a PbSe (444) spacing of 0.8837 Å, corresponding to a cubic lattice parameter of about 6.123 Å that is matched to the bulk.²⁶ The 2θ - ω full width at half maximum (FWHM) measured 442 arcsec, corresponding to approximately $\pm 0.06\%$ variability in (444) layer spacing. Rocking curve width was measured at 197 arcsec. These x-ray measurements are comparable to our previous work,¹⁶ PbSe/InAs(001) with an asymmetric (004) rocking curve width of 185 and 369 arcsec along the [110] and $[1\bar{1}0]$ azimuths, respectively. Other recent PbSe/III-V work from Wang *et al.*¹⁴ measured rocking curve widths of 266 and 1700 arcsec for PbSe/GaAs(001) and PbSe(511)/GaAs(211)B, respectively. High quality PbSe(111) on well-established fluorite buffer layers can reach rocking curve widths around 150 arcsec,²³ but 500–1500 arcsec is not uncommon.^{11,27} Extremely high quality PbTe has been grown on BaF₂ substrates with rocking curve width of only 30 arcsec.²⁸

The lattice mismatch between PbSe and InAs is accommodated by a dense triangular grid of misfit dislocations at the heterointerface. We have observed these misfits directly using the plan-view ECCI on a sloped, ion-polished sample of PbSe, where the misfit network is briefly shallow enough to generate channeling contrast [Fig. 4(b)]. Figure 4(c) shows the HAADF STEM of the PbSe/InAs interface with approximate positions of misfit dislocations marked. Across this 95 nm section, seven misfit dislocations are observed, resulting in an average spacing of ~ 14 nm. Misfit dislocations in these materials are expected to have burgers vectors in the $\langle 110 \rangle$ directions and glide on the $\{100\}$ planes. In a (111)-oriented film, this means that a triangular grid of misfit dislocations will lie at the heterointerface²²—each set with an equilibrium spacing of 30–40 nm. Because three discrete sets of dislocations exist, we would expect to see a dislocation intersect a [110] cross section every 17 nm, but in practice, direct observation and burgers circuit analysis are made difficult by the inclination of the dislocations to the imaging plane. Only half of the visible dislocations will be perpendicular to the imaging plane, and the rest are inclined at $\pm 60^\circ$, causing distortion and blurring at the interface in a foil of finite thickness. However, via masking and inverse fast Fourier transform analysis [Fig. 4(c) inset], approximate positions for dislocation cores can be determined.

As (111) is not the low-energy plane of these rocksalt materials, we noticed slightly rougher surfaces on these films than similar films grown on the (001) substrates. Interestingly, pits in the thin films of (001) PbSe¹⁶ seem to terminate on $\{111\}$ planes, but pits in the thin films of (111) PbSe seem to preferentially terminate on $\{001\}$ planes. Additionally, pits on (001) films seem to form around dislocations early in growth and later close to form a smooth surface, but in the (111) orientation, the opposite occurs. PbSe films can be very smooth immediately after coalescence and only develop shallow surface pits with very long growth. The density of these surface imperfections exceeds the density of threading dislocations at the film surface, so if these pits are indeed forming due to dislocations, this implies that dislocation glide in the relaxing film allows the same dislocation to nucleate multiple pits that persist.

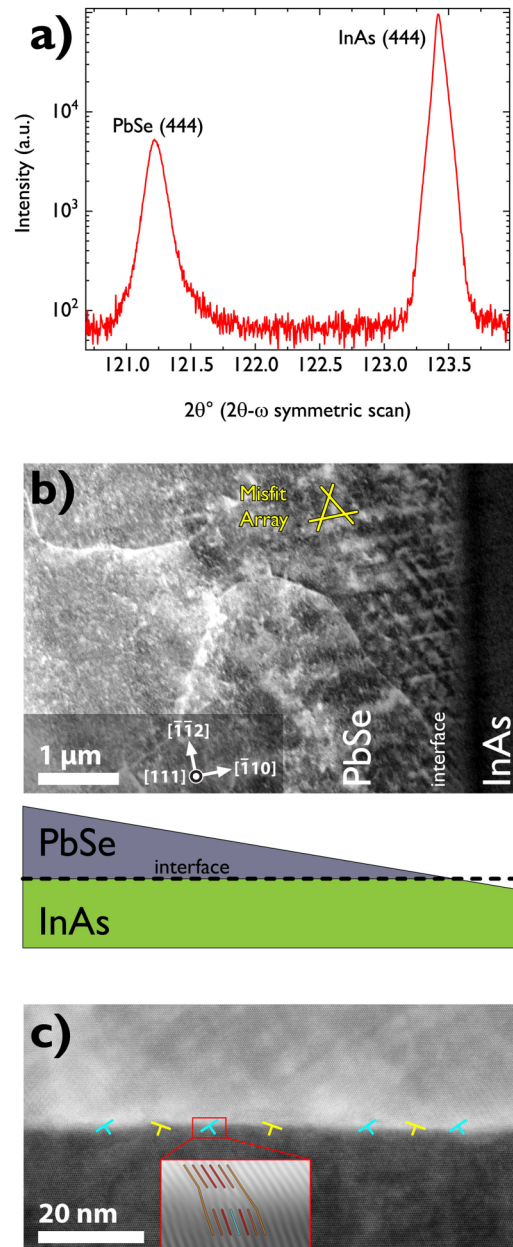


FIG. 4. Structural quality of a fully relaxed 1.5 μm thick PbSe film at room temperature: (a) Symmetric 2θ - ω XRD scan showing good structural quality, with a film FWHM of 442 arcsec. Rocking curve FWHM was 197 arcsec. (b) Plane-view ECCI micrograph of the FIB-polished sloped PbSe film, showing threading dislocations and twin boundaries in the thicker PbSe to the left, and a triangular array of misfit dislocations to the right where the film thickness approaches the ECCI interaction depth. The resolution of ECCI does not resolve every misfit dislocation. (c) shows the grid of misfit dislocations at the heterointerface, with approximate dislocation core positions determined through inverse fast Fourier transform analysis (c, inset). The tilted dislocation symbols indicate the two visible populations of dislocations, half perpendicular to the imaging plane, half inclined $\pm 60^\circ$ to the imaging plane.

D. Luminescence and recombination

Figure 5(a) shows high excitation spontaneous emission PL spectra from the 1.5 μm PbSe/InAs film collected from 83–300 K. Where conventional semiconductors increase in bandgap at low temperatures, PbSe is well-known to do the opposite.^{1,6} We also note in Fig. 5(a) that the emission intensity around room temperature is greater than that at cryogenic temperatures. We do not have a clear explanation for this at this time—there could be nonmonotonicity from competing temperature-dependent recombination lifetimes (discussed subsequently) or this may be an artifact of the PbSe/InAs interface. Regarding this latter point, none of the thinner samples (65 nm) of PbSe/InAs (111)A emit light that is characteristic of PbSe. It may be tempting to suggest that the network of misfit dislocations at the interface is responsible for the lack of photoluminescence from the thin PbSe films, but we do not think this is the case. When carriers in PbSe are contained by a larger bandgap substrate (i.e., a PbSe/GaAs structure), we have seen both (111)- and (001)-oriented PbSe emit light even for 50 nm thick films, in spite of an 8% lattice mismatch and a very dense network of misfit dislocations. We will discuss these results on larger bandgap substrates elsewhere. InAs has a similar narrow bandgap to PbSe at room temperature, and while the band alignment between PbSe and InAs(111)A across this type B epitaxial interface is not known, we anticipate a type-III alignment as in the case of PbTe/InSb.¹⁵ This suggests that in the thinner samples, photogenerated carriers may diffuse into the InAs substrate before radiatively recombining. More work is needed to understand whether the luminescence intensity in the 1.5 μm film is characteristic of bulk behavior or is influenced by the heterostructure, especially at cryogenic temperatures where photogenerated carriers may be highly mobile.

Figure 5(b) shows the PL-calculated bandgap as the sample temperature is changed. Due to thermal mismatch with the InAs substrate ($\alpha_{\text{InAs}} = 4.5 \times 10^{-6} \text{ K}^{-1}$, $\alpha_{\text{PbSe}} = 19.4 \times 10^{-6} \text{ K}^{-1}$),^{26,29} the PbSe layer should be significantly biaxially tensile strained (0.7%) while cooling from 573 K growth temperature to 83 K. Yet, a closer inspection of the temperature dependence of the thin film bandgap as derived from PL spectra highlights the remarkable ability of these films to stay relaxed due to dislocation glide even at cryogenic temperatures. In contrast, III-V/Si(001) films do not experience thermal dislocation glide below 200–300 °C and routinely crack upon cool down, even with substantially smaller thermal mismatch.³⁰ The bandgap of the PbSe film reduces approximately linearly with temperature ($\sim 0.48 \text{ meV/K}$), in excellent agreement with the unstrained bulk PbSe bandgap.¹ Hypothetically, if dislocation glide did not take place, the elastic (111) biaxial strain would break the star-degeneracy of the normal and oblique $\langle 111 \rangle$ direct L-valley gaps, shifting them dissimilarly (strictly leading to an indirect semiconductor) as well as widening them, the [111] L-valley (normal) forming the smallest direct gap.^{31–33} Figure 5(b) shows this splitting and increase in the bandgap for two hypothetical elastically strained PbSe films: one all the way down from the growth temperature and the other only from room temperature and below.

Complementary to continuous-wave PL measurements, TRPL and power-dependent photoluminescence (PDPL) (Fig. 6) allow for the probing of minority carrier recombination in the 1.5 μm PbSe

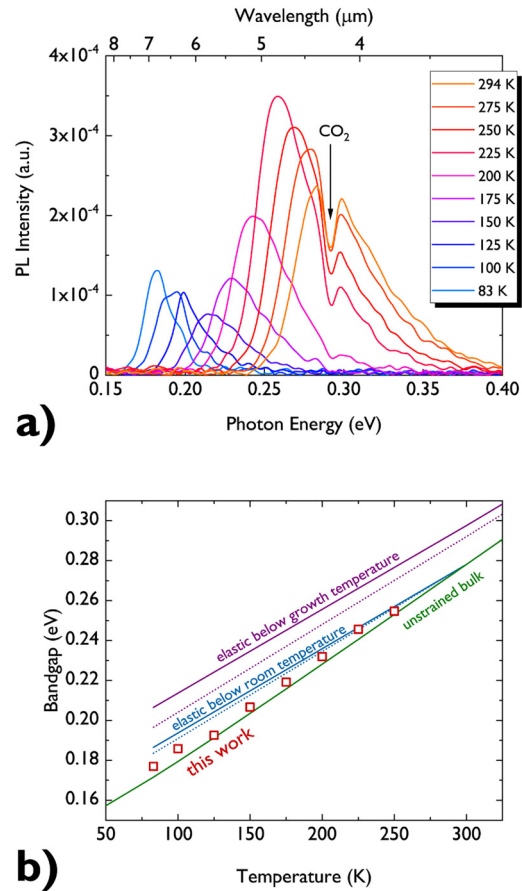


FIG. 5. Temperature-dependent bandgap derived from photoluminescence: (a) Photoluminescence spectra of 1.5 μm PbSe/InAs between room temperature and 83 K, showing the decrease in bandgap and peak broadness with temperature. The room-temperature spectrum is interrupted by absorption from atmospheric CO_2 . (b) Bandgap is plotted against temperature, showing a near-linear decrease in bandgap with temperature, in rough agreement with anticipated bulk PbSe (Ref. 1). For point of comparison, the higher lines show hypothetical bandgaps from strained PbSe films calculated from deformation potentials (Ref. 31). The solid lines represent the [111] L-valley gaps, and the dotted lines represent the oblique L-valley gaps.

film. In the low-injection regime at room temperature, the TRPL intensity is seen to decay (single) exponentially over nearly two orders of magnitude after photoexcitation. From this, we calculate a recombination lifetime of 20 ns. A faster pump-power-dependent recombination pathway is apparent in the early stages of decay, when the excitation becomes comparable to the background doping in the sample. Making the bold assumption that the luminescence from PbSe/InAs is characteristic of bulk behavior, the low-injection minority carrier lifetime τ_{eff} can be ascribed to radiative and nonradiative recombination occurring in parallel,

$$\tau_{\text{eff}} = \frac{1}{\tau_{\text{SRH}}} + \frac{1}{\tau_{\text{Rad}}} + \frac{1}{\tau_{\text{Auger}}}, \quad (1)$$

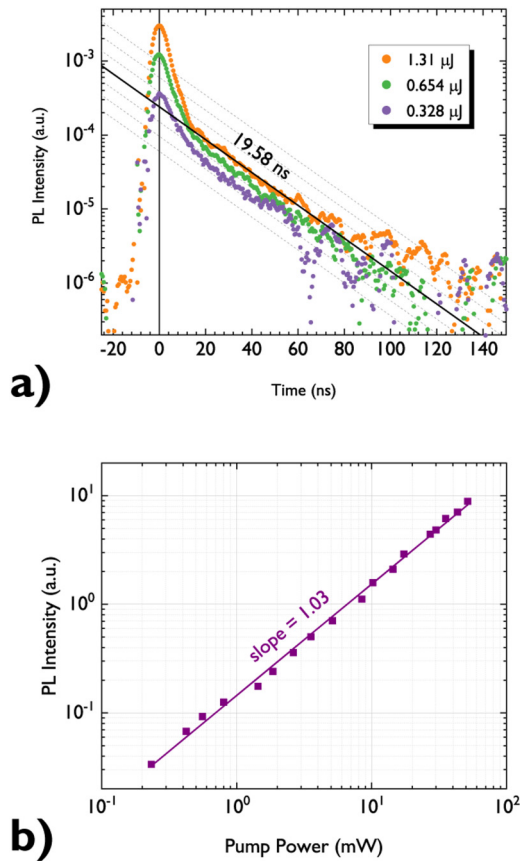


FIG. 6. Recombination characteristics from PL at room temperature: (a) TRPL: Three different pumping intensities (all more than an order of magnitude below the PL above) produce photoexcited carriers that recombine over the span of about 100 ns. By fitting to the single exponential region of this data, a minority carrier lifetime of approximately 20 ns can be calculated, given by the slope of the black line. (b) PDPL: PL Intensity is seen to scale directly with pump power over a 220× range with an exponent of 1.03, characteristic of a “z = 2” process like bimolecular e-h pair radiative recombination.

where τ_{SRH} is the nonradiative Shockley-Read-Hall (SRH) lifetime, τ_{Rad} is the radiative lifetime, and τ_{Auger} is nonradiative bulk Auger recombination lifetime.³⁴ Typically, recombination in room-temperature PbSe is reported to be Auger-dominated,^{35,36} so we first consider the contribution of e-e-h τ_{Auger} , calculated as

$$\tau_{Auger} = \frac{1}{Cn_0^2}, \quad (2)$$

where C is the Auger recombination coefficient and n_0 is the doping density.³⁴ We are not able to measure actual carrier concentration in these films due to the conductive InAs substrates, but nonstoichiometry-induced n-type doping of $1-5 \times 10^{17} \text{ cm}^{-3}$ is typically expected in films evaporated from a compound PbSe cell without excess Se-flux.³⁷ Indeed, exceeding this electron

concentration would result in lead droplets on the film that we did not observe. Recent first principles calculations by Zhang *et al.* place the Auger coefficient C for PbSe with $5 \times 10^{17} \text{ cm}^{-3}$ carriers at approximately $4 \times 10^{-29} \text{ cm}^6 \text{ s}^{-1}$, just slightly lower than that measured experimentally by Klann *et al.* and Findlay *et al.*³⁸⁻⁴⁰ This yields a bulk Auger lifetime of ~ 100 ns, barely within an order of magnitude of the effective lifetime of 20 ns we observe.

PDPL measurements [Fig. 6(b)], on the other hand, indicate a process with bimolecular power dependence. A power law fit shows PL intensity rising with pump power with an exponent of 1.03 over two orders of magnitude in excitation intensity, where we would expect $\frac{2}{3}$ for conventional e-e-h Auger recombination dominated (rate $\rho \propto n^2p$), 1 for radiative recombination dominated (rate $\propto np$), or 2 for SRH recombination dominated (rate $\propto p$). This suggestion of radiative recombination is surprising as τ_{Rad} in PbSe has been calculated to be approximately 150 ns at $n_0 = 5 \times 10^{17} \text{ cm}^{-3}$ at room temperature³⁶—also far too slow to explain the measured τ_{eff} . Photon recycling effects make this estimate of τ_{Rad} less meaningful as only a small fraction of the light escapes the PbSe film due to the very high index of refraction, causing τ_{Rad} to appear even slower.⁴¹ Haug lists cases involving degenerate doping where the direct Auger recombination rate may show a rate $\propto np$ dependence.⁴² Mocker and Ziep also calculate strong deviations of the rate $\propto n^2p$ of the Auger process toward a rate $\propto np$ at very high excitation in lead chalcogenides (non-equilibrium carriers exceeding 10^{19} cm^{-3}),⁴³ and similar observations have been made in indium nitride and the zincblende III-V materials.^{44,45} Going forward, a set of samples with controlled impurity doping would help shed light on this issue.

Finally, we mention one additional type of Auger process previously mentioned in the context of polycrystalline IV-VI thin films: impurity or trap-assisted Auger recombination (TAAR).⁴⁶ TAAR, like radiative recombination, yields a recombination rate $\propto np$ and should lead to low quantum efficiency films where the luminescence intensity nevertheless scales linearly with pump power.⁴⁷ In order to confirm the presence of such a mechanism, we would like to both measure the quantum efficiency of the samples as well as note for luminescence to scale with the concentration of a measurable defect in future work. We explore the unlikely case that lifetime is dominated by SRH recombination in Sec. IV B.

IV. DISCUSSION

A. Formation of type-B interfaces

In this work, we have explored PbSe growth on a (111)A III-V surface, showing that a consistent crystallographic rotation of 180° results from a high-temperature PbSe pretreatment. The ability to prepare a surface for growth via a high temperature surface treatment is not new in IV-VI epitaxy. We have previously explored cube-on-cube growth of (001) PbSe on (001) III-V substrates using a high-temperature dose of PbSe,¹⁶ and other groups previously explored alternate orientations, showing that (211) oriented GaAs substrates prepared under a chalcogenide overpressure can controllably nucleate (511)-oriented PbSe films.¹⁴ With any epitaxial growth, the ideal surface acts as a template for ordered nucleation, and in these cases, it appears that a high-temperature pretreatment with IV-VI or VI flux can aid in producing such a template. The

high temperature, above the re-evaporation temperature for PbSe, ensures that no film can actually grow while the surface is still rearranging and provides the kinetic freedom for the surface to find a minimum-energy configuration.

Specifically, in the case of rotational twins on the (111) plane, varied atomic stackings can have extremely similar energies, and here, these minor changes coincide with what is already an extremely energetically expensive heterovalent interface. PbTe and PbSe, similar in structure and bonding, have been observed to form both type A and type B interfaces on different (111) substrates. On bare Si(111), PbTe forms an unrotated type A interface,¹¹ but on BaF₂ substrates and buffer layers, the favored epitaxial arrangement for PbSe and PbTe is type B.⁴⁸ Hohnke *et al.* explain that this rotation is due to nearest- and second-nearest- neighbor effects across the heterointerface and believe that the type-B stacking is thermodynamically favorable. On zincblende CdTe(111), results are mixed. PbTe typically forms a type A interface on CdTe but has been observed to form a type B interface under certain situations. The authors attribute this phenomenon to a non-equilibrium growth mode, as DFT actually indicates that the type B interface is more energetically expensive by a slim margin of about 12.5 meV/atom.⁴⁹

The problem of variable interfacial stacking is not limited to IV-VI films—type B interfaces have also been observed in the Ge/CaF₂ system,⁵⁰ a covalent diamond cubic film on a fluorite substrate, and the CoSi₂/Si system,⁵¹ a metal fluorite film on a diamond cubic substrate. In the case of Ge/CaF₂, the energy difference between stackings is less than 10 meV/atom.⁵⁰ This very narrow energy difference results in a slight preference toward the type B interface that increases at higher temperatures. The authors also point to the removal of the top fluorine layer of the substrate as critical for forming the type B stacking. In this case, as with the IV-VI examples, it appears that the placement of the first monolayer of atoms past the heterointerface is critical to set epitaxial symmetry for the rest of the growing film.

In the case of the present work, we believe that our high-temperature surface treatment creates what amounts to one monolayer of zincblende-oriented PbSe. Above, we explained this as a displacement of the structural interface from the chemical interface, but the chemical interface may itself not be perfectly abrupt. Before the PbSe dose, in RHEED, we observe a 2 × 2 reconstruction on the InAs surface, which could indicate an arsenic trimer structure and as much as ¾ of a monolayer of arsenic remaining. During the PbSe dose, it is likely that not all of this residual arsenic is evaporated, resulting in a mixed composition layer. Such a mixed selenium-arsenic layer would have a much stronger bias toward tetrahedral bonding when in the presence of an existing zincblende film. After the PbSe dose, we see a 1 × 1 RHEED pattern, which we believe corresponds to an unreconstructed pseudozincblende lead-terminated surface.

This PbSe dosing procedure occurs at 400 °C, so the thermal energy available to adatoms is on the order of 60 meV (k_BT), but differences in stacking energies reported for PbTe/CdTe and Ge/CaF₂ are only on the order of 10–15 meV/atom. If these energies were the only relevant scales, we would expect a nearly random distribution of both stackings. However, these reported energetic differences are for interfaces between two slabs of material, not the stacking at a surface. With only a single monolayer of

material deposited on a substrate during the pretreatment, we find this procedure essentially 100% effective at regulating stacking. Necessarily then, the selective driving force for type B stacking must be much higher than k_BT during the treatment to cause such an extreme bias. There may also be a rapid ripening process that results in a single-orientation film across the wafer after initial nucleation, but if such a ripening process does contribute, we know it is limited by the underlying structure—as in Fig. 3. The PbSe does not form a continuous layer of the majority stacking; instead, it conforms closely to the twinned regions that already exist in the buffer.

B. Recombination and defect tolerance

Despite being able to control island orientation, the process of island coalescence still produces many threading dislocations. In III-V and II-VI infrared-active semiconductors, an average TDD of ~1 × 10⁸ would severely compromise the luminescence properties via SRH recombination. We can obtain an upper bound for the dislocation recombination activity by *assuming* that the measured lifetime is SRH limited and comparing to a simple model where dislocations are infinitely strong recombination sinks for minority carriers. Yamaguchi *et al.* use this model to calculate the effect of threading dislocations on the SRH lifetime in GaAs,^{52,53}

$$\frac{1}{\tau_{SRH}} = \frac{\pi^3 D_p N_d}{4} \quad (3)$$

D_p is the minority carrier (hole) diffusion coefficient and N_d is the TDD. This model works satisfactorily for III-V semiconductors.^{54–56} The hole mobility in bulk PbSe at 300 K has been measured to be roughly 300 cm²/V s,⁵⁷ which yields a D_p of 7.8 cm²/s. Even for a best-case surface TDD of 1 × 10⁸ cm⁻², this simple model suggests τ_{SRH} = 170 ps. Considering the measured total effective lifetime in these samples is 120× longer, the recombination activity of dislocations (and the surface) in PbSe appears to be low compared to III-V materials, and this is a conservative estimate. Detailed verification of this will require the ability to tune the TDD in the film as has been done for III-V/Si samples. For an experimental point of comparison to other IR material systems, MBE-grown Hg_{0.22}Cd_{0.78}Te with EPD of 10⁸/cm² is reported to have a dislocation-limited minority carrier lifetime of about 15 ns only at 78 K,⁵⁸ similar to our results at room temperature.

This outstanding dislocation-tolerant behavior in PbSe, perhaps, should not be surprising given accounts of greatly reduced surface recombination velocities in the IV-VIs^{59,60} and very early demonstrations of lasing.^{61,62} The lack of SRH recombination has often been attributed to high static dielectric constants or partitioned bonding allowing for the screening of charged defects,⁶ although more recent work has called into question the true nature of bonding in IV-VI materials.^{7–9} Cahen *et al.*⁷ point to the character of covalency in PbSe to explain defect tolerant behavior, drawing parallels to the methylammonium lead halide material system. The distinction between bonding and antibonding covalency could govern both the material polarizability and the absolute position of defect states and relevant bands. We hope that studies on carrier capture coefficients⁶³ at simple defects in PbSe may shed

light on this issue. At the same time, we should not discount more mundane mechanisms of impurity passivation of surfaces and defects.⁶⁴

V. SUMMARY AND CONCLUSIONS

In this work, we examined the high-energy heteroepitaxial interface between PbSe(111) and InAs(111)A and determined that consistent single-orientation nucleation is achievable. By exposing an InAs surface to the PbSe flux at a temperature above the re-evaporation limit for PbSe, we quickly convert the surface into a suitable template for growth of PbSe(111) without nanoscale rotated/mirrored grains. We believe this procedure slightly separates the structural and chemical interfaces, forming a uniform 180° rotational twin across the entire interface between the substrate and film. As multinucleation of type A and type B islands results in an extremely high concentration of defects in a film [grain boundaries in Fig. 1(a)], the ability to reliably control this process is a necessary first step toward device-quality (111) IV-VI/III-V films.

Growing in the (111) orientation enables access to the extremely active primary slip system of rocksalt PbSe. Not only does this allow for glide, rapid dislocation annihilation, and crack-free cooldown, but the temperature-tunable bandgap of bulk PbSe creates the opportunity for tunable optoelectronic devices where the active IV-VI layer would always be relaxed. However, future work will need to address the effect of alloying on the motion of these dislocations. Using alloys like PbSnSe, PbGeSe, or SnGeSe in nominally PbSe-based devices could be very fruitful from the perspective of device design, but alloy hardening and the addition of extra mismatched interfaces may result in less effective glide. The performance of standard semiconductor growth techniques like cyclic thermal annealing, graded buffers, and dislocation filtering layers has yet to be determined.

Even with a finite number of twin boundaries and quite high TDDs, we observe strong light emission and long minority carrier lifetimes from the PbSe layer. The 20 ns lifetime we observe is dominated by a recombination mechanism with radiative-like bimolecular power dependence, but based on previous calculations, we doubt these films are radiatively limited. Auger recombination has been observed with radiative-like power dependence in cases of carrier degeneracy at high pumping, or with the consideration of trap-assisted processes, and we tentatively attribute recombination in these films to one of these Auger mechanisms. These thin films are on a narrow-gap substrate, and the influence of the substrate and band offset on carrier diffusion and recombination is not yet known. Overall, the relatively long lifetime and emission of light from these samples despite high TDD implies that these materials are not SRH limited, and this shows promise for future optoelectronic devices with a significant degree of defect tolerance.

ACKNOWLEDGMENTS

The authors would like to express their gratitude to Art Gossard for his leadership in the science and technology of MBE and, in particular, for teaching and inspiring generations of scientists through the activities of the MBE lab at UC Santa Barbara. This work was supported through the National Science Foundation

(NSF) Materials Research Science and Engineering Center (MRSEC) at UC Santa Barbara: No. NSF DMR-1720256 (Seed program). We also acknowledge the use of shared facilities of the NSF MRSEC at UC Santa Barbara (No. DMR 1720256). B.B.H. acknowledges support from the National Science Foundation Graduate Research Fellowship under Grant No. 1650114. K.M. acknowledges support from the National Science Foundation CAREER Award under Grant No. DMR-1945321 and thanks Xie Zhang and Chris Van de Walle for helpful discussions on Auger recombination in PbSe. L.N. and D.W. acknowledge support from the National Science Foundation under Grant No. ECCS-1926187. K.D.H. and P.J.S. acknowledge support from the College of Engineering at Boise State University. We also would like to acknowledge Kurt Olsson and John English for their MBE expertise and support.

DATA AVAILABILITY

The data that support the findings of this study are available from the corresponding author upon reasonable request.

REFERENCES

- ¹H. Preier, *Appl. Phys.* **20**, 189 (1979).
- ²H. Zogg, A. Fach, J. John, P. Mueller, and C. Paglino, in *SPIE 1996 International Symposium on Optical Science, Engineering, and Instrumentation*, edited by R. E. Longshore and J. W. Baars, Denver, CO, 22 October 1995 (SPIE, 1995), pp. 35–42.
- ³G. Springholz, T. Schwarz, W. Heiss, G. Bauer, M. Aigle, H. Pascher, and I. Vavra, *Appl. Phys. Lett.* **79**, 1225 (2001).
- ⁴M. Fill, A. Khair, M. Rahim, F. Felder, and H. Zogg, *J. Appl. Phys.* **109**, 093101 (2011).
- ⁵H. Zogg, A. Fach, C. Maissen, J. Masek, and S. Blunier, *Opt. Eng.* **33**, 1440 (1994).
- ⁶G. Springholz and G. Bauer, *Wiley Encyclopedia of Electrical and Electronics Engineering* (John Wiley & Sons, Inc., Hoboken, NJ, 2014), pp. 1–16.
- ⁷Y. Rakita, T. Kirchartz, G. Hodes, and D. Cahen, “Type and degree of covariance: Empirical derivation and implications,” [arXiv.org/abs/1907.03971](https://arxiv.org/abs/1907.03971) (2019).
- ⁸J. Raty, M. Schumacher, P. Golub, V. L. Deringer, C. Gatti, and M. Wuttig, *Adv. Mater.* **31**, 1806280 (2019).
- ⁹S. Maier *et al.*, *Adv. Mater.* **32**, 2005533 (2020).
- ¹⁰H. Zogg, P. Mueller, A. Fach, J. John, C. Paglino, and A. N. Tiwari, in *SPIE 1995 International Symposium on Optical Science, Engineering, and Instrumentation*, edited by R. E. Longshore, J. W. Baars, A. Kepten, and J. M. Trombetta, San Diego, CA, 1 September 1995 (SPIE, 1995), pp. 35–42.
- ¹¹P. Müller, A. Fach, J. John, A. N. Tiwari, H. Zogg, and G. Kostorz, *J. Appl. Phys.* **79**, 1911 (1996).
- ¹²P. J. McCann, I. Chao, H. Sachar, D. McAlister, C. Li, X. Fang, H. Wu, and K. Namjou, *Spectrochim. Acta Part A Mol. Biomol. Spectrosc.* **55**, 1999 (1999).
- ¹³X. L. Huang, Z. Labadi, A. Hammiche, and A. Krier, *J. Phys. D Appl. Phys.* **35**, 3091 (2002).
- ¹⁴X. J. Wang, Y. B. Hou, Y. Chang, C. R. Becker, R. F. Klie, T. W. Kang, R. Sporcken, and S. Sivanathan, *J. Cryst. Growth* **311**, 2359 (2009).
- ¹⁵K.-K. Lee, W. Priyantha, and T. H. Myers, *Appl. Phys. Lett.* **100**, 052108 (2012).
- ¹⁶B. B. Haidet, E. T. Hughes, and K. Mukherjee, *Phys. Rev. Mater.* **4**, 033402 (2020).
- ¹⁷J. Yoshino, H. Munekata, and L. L. Chang, *J. Vac. Sci. Technol. B* **5**, 683 (1987).
- ¹⁸H. Clemens, H. Krenn, B. Tranta, P. Ofner, and G. Bauer, *Superlattices Microstruct.* **4**, 591 (1988).

- ¹⁹B. Zhang, P. Lu, H. Liu, L. Jiao, Z. Ye, M. Jaime, F. F. Balakirev, H. Yuan, H. Wu, W. Pan, and Y. Zhang, *Nano Lett.* **15**, 4381 (2015).
- ²⁰M. B. Lassise, T. T. McCarthy, B. D. Tracy, D. J. Smith, and Y.-H. Zhang, *J. Appl. Phys.* **126**, 045708 (2019).
- ²¹Y. Kamimura, K. Edagawa, and S. Takeuchi, *Acta Mater.* **61**, 294 (2013).
- ²²P. Müller, H. Zogg, A. Fach, J. John, C. Paglino, A. N. Tiwari, M. Krejci, and G. Kostorz, *Phys. Rev. Lett.* **78**, 3007 (1997).
- ²³H. Zogg *et al.*, *Phys. Rev. B* **50**, 10801 (1994).
- ²⁴K. D. Vallejo, T. A. Garrett, K. E. Sautter, K. Saythavy, B. Liang, and P. J. Simmonds, *J. Vac. Sci. Technol. B* **37**, 061810 (2019).
- ²⁵G. Springholz and G. Bauer, *J. Appl. Phys.* **77**, 540 (1995).
- ²⁶O. Madelung, U. Rössler, and M. Schulz, *Non-Tetrahedrally Bonded Elements and Binary Compounds I* (Springer-Verlag, Berlin, 1998), pp. 1–4.
- ²⁷C. P. Li, P. J. McCann, and X. M. Fang, *J. Cryst. Growth* **208**, 423 (2000).
- ²⁸G. Springholz, G. Bauer, and G. Ihninger, *J. Cryst. Growth* **127**, 302 (1993).
- ²⁹O. Madelung, U. Rössler, and M. Schulz, *Group IV Elements, IV–IV, and III–V Compounds. Part a—Lattice Properties* (Springer-Verlag, Berlin, 2001), pp. 1–6.
- ³⁰V. K. Yang, M. Groenert, C. W. Leitz, A. J. Pitera, M. T. Currie, and E. A. Fitzgerald, *J. Appl. Phys.* **93**, 3859 (2003).
- ³¹I. I. Zasavitskii, E. A. de Andrada e Silva, E. Abramof, and P. J. McCann, *Phys. Rev. B* **70**, 115302 (2004).
- ³²J. R. Burke and G. P. Carver, *Phys. Rev. B* **17**, 2719 (1978).
- ³³D. Genzow, M. Mocker, and E. Normantas, *Phys. Status Solidi* **135**, 261 (1986).
- ³⁴M. Grundmann, *The Physics of Semiconductors* (Springer, Berlin, 2010).
- ³⁵O. Ziep, D. Genzow, M. Mocker, and K. H. Herrmann, *Phys. Status Solidi* **99**, 129 (1980).
- ³⁶H. Zogg, W. Vogt, and W. Baumgartner, *Solid State Electron.* **25**, 1147 (1982).
- ³⁷D. K. Hohnke and S. W. Kaiser, *J. Appl. Phys.* **45**, 892 (1974).
- ³⁸X. Zhang, J.-X. Shen, and C. G. Van de Walle, *Phys. Rev. Lett.* **125**, 037401 (2020).
- ³⁹R. Klann, T. Hofer, R. Buhleier, T. Elsaesser, and A. Lambrecht, *Semicond. Sci. Technol.* **8**, S305 (1993).
- ⁴⁰P. C. Findlay *et al.*, *Phys. Rev. B* **58**, 12908 (1998).
- ⁴¹R. K. Ahrenkiel, D. J. Dunlavy, B. Keyes, S. M. Vernon, T. M. Dixon, S. P. Tobin, K. L. Miller, and R. E. Hayes, *Appl. Phys. Lett.* **55**, 1088 (1989).
- ⁴²A. Haug, *Solid State Electron.* **21**, 1281 (1978).
- ⁴³M. Mocker and O. Ziep, *Phys. Status Solidi* **115**, 415 (1983).
- ⁴⁴J. Hader, J. V. Moloney, and S. W. Koch, *Appl. Phys. Lett.* **87**, 201112 (2005).
- ⁴⁵A. McAllister, D. Bayer, and E. Kioupakis, *Appl. Phys. Lett.* **112**, 251108 (2018).
- ⁴⁶J. Vaitkus, M. Petrauskas, R. Tomašiūnas, and R. Masteika, *Appl. Phys. A Solids Surfaces* **54**, 553 (1992).
- ⁴⁷D. J. Myers, A. C. Espenlaub, K. Gelzinyte, E. C. Young, L. Martinelli, J. Peretti, C. Weisbuch, and J. S. Speck, *Appl. Phys. Lett.* **116**, 091102 (2020).
- ⁴⁸D. K. Hohnke, H. Holloway, and M. D. Hurley, *Thin Solid Films* **38**, 49 (1976).
- ⁴⁹S. Jin, C. Cai, B. Zhang, H. Wu, G. Bi, J. Si, and Y. Zhang, *New J. Phys.* **14**, 113021 (2012).
- ⁵⁰T.-L. Chan, C. Gaire, T.-M. Lu, G.-C. Wang, and S. B. Zhang, *Surf. Sci.* **604**, 1645 (2010).
- ⁵¹J. M. Gibson, R. T. Tung, J. M. Phillips, and J. M. Poate, *MRS Proc.* **25**, 405 (1983).
- ⁵²M. Yamaguchi and C. Amano, *J. Appl. Phys.* **58**, 3601 (1985).
- ⁵³M. Yamaguchi, A. Yamamoto, and Y. Itoh, *J. Appl. Phys.* **59**, 1751 (1986).
- ⁵⁴C. L. Andre, J. J. Boeckl, D. M. Wilt, A. J. Pitera, M. L. Lee, E. A. Fitzgerald, B. M. Keyes, and S. A. Ringel, *Appl. Phys. Lett.* **84**, 3447 (2004).
- ⁵⁵R. K. Ahrenkiel, M. M. Al-Jassim, D. J. Dunlavy, K. M. Jones, S. M. Vernon, S. P. Tobin, and V. E. Haven, *J. Electrochem. Soc.* **137**, 3 (1990).
- ⁵⁶R. K. Ahrenkiel, T. Wangensteen, M. M. Al-Jassim, M. Wanlass, and T. Coutts, *AIP Conf. Proc.* **321**, 412–424 (1995).
- ⁵⁷J. Si, H. Wu, T. Xu, and C. Cao, *J. Zhejiang Univ. A* **9**, 137 (2008).
- ⁵⁸S. H. Shin, J. M. Arias, M. Zandian, J. G. Pasko, and R. E. DeWames, *Appl. Phys. Lett.* **59**, 2718 (1991).
- ⁵⁹Z. Shi, *Appl. Phys. Lett.* **72**, 1272 (1998).
- ⁶⁰A. Pinto Neto, H. Vargas, N. F. Leite, and L. C. M. Miranda, *Phys. Rev. B* **40**, 3924 (1989).
- ⁶¹J. F. Butler, A. R. Calawa, R. J. Phelan, A. J. Strauss, and R. H. Rediker, *Solid State Commun.* **2**, 303 (1964).
- ⁶²J. F. Butler, A. R. Calawa, R. J. Phelan, T. C. Harman, A. J. Strauss, and R. H. Rediker, *Appl. Phys. Lett.* **5**, 75 (1964).
- ⁶³X. Zhang, M. E. Turiansky, and C. G. Van de Walle, *J. Phys. Chem. C* **124**, 6022 (2020).
- ⁶⁴F. Zhao, S. Mukherjee, J. Ma, D. Li, S. L. Elizondo, and Z. Shi, *Appl. Phys. Lett.* **92**, 211110 (2008).